Ab initio studies of high-pressure transformations in GeO_2

Z. Łodziana and K. Parlinski
Institute of Nuclear Physics, ul. Radzikowskiego 152, 31-342 Kraków, Poland

J. Hafner
Institute for Materials Physics, University of Vienna, Sensengasse 8/12, A-1090 Vienna, Austria
(Received 26 June 2000; revised manuscript received 23 October 2000; published 7 March 2001)

We performed *ab initio* calculations of germanium dioxide to study its behavior and possible similarity to silica under high pressure. At the rutile-$CaCl_2$-type phase transition, the lattice constants, unit cell volume, and Gibbs free energy change continuously with increasing pressure and indicate that this ferroelastic phase transition is close to the second order. Further phase transitions to denser packed phases of α-PbO_2-type and pyrite $Pa\bar{3}$ are considered. The pressure dependence of the elastic constants is determined. For zero-pressure and 30-GPa phonon dispersion relations of rutile-type and $CaCl_2$-type structures, respectively, are calculated. A softening of an optical mode, linearly coupled to a shear instability, is found. The present results confirm the analogy of the phase-transition sequence between silica and germanium dioxide at high pressures.

DOI: 10.1103/PhysRevB.63.134106 PACS number(s): 62.50.+p, 71.15.Mb, 63.20.−e

I. INTRODUCTION

The great interest in the high pressure phase transitions in silica SiO_2 comes from the possible geophysical repercussions. The high pressure polymorphs of silica have been studied quite intensively.[1–6] The α-quartz structure, which is the silica polymorph stable at ambient conditions, transforms to the coesite phase at around 3 GPa. Then, above 9 GPa coesite transforms into the stishovite phase. At higher pressure silica shows a sequence of phase transitions:[7,8] stishovite (rutile) $(P4_2/mnm,\ Z=2)\Rightarrow(\sim 50$ GPa) $\Rightarrow CaCl_2$-type $(Pnnm,Z=2)\Rightarrow(\sim 85$ GPa) $\Rightarrow\alpha$-PbO_2-type $(Pbcn,Z=4)\Rightarrow(\sim 205$ GPa) $\Rightarrow$pyrite (modified fluorite)-type $(Pa\bar{3},Z=4)$. The tetragonal stishovite phase transforms reversibly to an orthorhombic, $CaCl_2$-type phase.[1,3,8–10] According to Landau theory this phase transition should be ferroelastic and of second order. It involves the softening of the Raman active B_{1g} mode. The softening of the B_{1g} mode has been confirmed experimentally.[1] This soft mode becomes an A_g mode in the orthorhombic phase. Under higher pressures silica transforms to post-stishovite phases, like α-PbO_2,[2] pyrite. For the stability range of α-PbO_2-type phase, on the basis of the density functional theory calculations, Teter *et al.*[7] proposed a large class of energetically competitive phases that could be generated from hcp arrays of oxygen with silicon occupying one-half of the octahedral sites. The high-pressure phase transitions in silica, however, present experimental problems as they occur well above the solidification pressure of all transmitting media.

In tin dioxide SnO_2, a similar series of phase transitions, rutile-type $(P4_2/mnm,Z=2)\Rightarrow(\sim 11.8$ GPa) $\Rightarrow CaCl_2$-type $(Pnnm,Z=2)\Rightarrow(\sim 15$ GPa) $\Rightarrow\alpha$-PbO_2-type$(Pbcn,Z=4)\Rightarrow(\sim 21$ GPa) $\Rightarrow$pyrite (modified fluorite)-type $(Pa\bar{3},Z=4)$ was measured.[11] The phase transition to the α-PbO_2-phase was observed under increasing pressure, and only part of the sample was transformed. The rutile-$CaCl_2$-type phase transition proved to be ferroelastic and should be accompanied by a soft mode.[12] Similar behavior is expected for PbO_2 (see Ref. 13).

Thus the interest can be focused on the investigation of the silica analog GeO_2,[14,15] which undergoes the same series of rutile-type to $CaCl_2$-type phase transitions at lower pressures. GeO_2 has structural properties very close to SiO_2 and SnO_2. Moreover, GeO_2 is considered to display the high-pressure properties of silica at relatively moderate pressures and thus is more easily accessible to the experimental investigations.[15] At ambient pressure GeO_2 exists in the rutile-type structure. Raman experiments[16] indicate that this compound transforms at 26.7 GPa from rutile-type to the $CaCl_2$-type structure and that the phase transition is of second order. Note that at ambient pressure SiO_2 has the α-quartz structure, while GeO_2 exists in the rutile-type symmetry. A quartzlike structure of germanium dioxide can be obtained only at high pressure and temperatures above 1000 K.

There exist a wide literature on the low pressure behavior of germanium dioxide,[17–20] but information on the possible existence of post-stishovite phases in GeO_2 is scarce. In particular, there is no confirmation that GeO_2 undergoes the same series of phase transitions under pressure as SiO_2 (silica) or SnO_2 do.

In the present paper we report on detailed *ab initio* calculations of the rutile-$CaCl_2$ phase transition. The possible phase transitions to α-PbO_2 and the pyrite structure and the relative stability of some post-stishovite phases are also considered. In the following paragraph we present the method of calculations, then in Sec. III the structural properties and changes arising under increasing pressure are presented. In Sec. IV we calculate phonon dispersion relations of the rutile-type and $CaCl_2$-type phases and the pressure dependence of the Raman active modes. In Sec. V we treat the pressure behavior of the elastic constants. The paper is completed with the conclusions.

II. METHOD

The *ab initio* calculations of GeO_2 were performed within the density functional theory, using the pseudopotential

TABLE I. Calculated structural parameters of GeO_2. For each phase the pressure is given in GPa, at which the calculations are done. Lattice constants are in Å.

Phase	Space group	Pressure	Lattice	Constants	Atomic positions
Rutile-type	$P4_2/mnm$	0	a	4.3838	Ge:(0,0,0)
(Stishovite)	$Z=2$		c	2.8637	O:(x,x,0)
Tetragonal					$x=3059$
$CaCl_2$-type	$Pnnm$	30	a	4.2813	Ge:(0.0,0.0,0.0)
Orthorhombic	$Z=2$		b	4.1430	O:(0.3229,0.2833,0.0)
			c	2.7984	
α-PbO_2-type	$Pbcn$	40	a	4.5792	Ge:(0.5,0.6613,0.25)
Orthorhombic	$Z=4$		b	4.0956	
			c	5.0880	O:(0.2394,0.8920,0.4221)
Pyrite-type	$Pa\bar{3}$	70	a	4.4046	Ge:(0.0,0.0,0.0)
Cubic	$Z=4$				O:(x,x,x)
					$x=0.3473$

method with the local density approximation (LDA) implemented in the VASP package.[21,22] It is generally believed that the gradient corrected methods should give more accurate results as to pressure behavior of crystals. LDA method, however, has proven to give very reasonable results of structural parameters, elastic constants, and transition pressures, as applied to the SiO_2 (Refs. 7,23) unless one compares tetrahedraly and octahedraly coordinated Si (or Ge), thus we do not go beyond this approach. Vanderbilt-type ultrasoft pseudopotentials, provided by the package, were used for germanium and oxygen. These pseudopotentials represent s^2p^2 and s^2p^4 electron configurations of Ge and O atoms, respectively. For Ge the $4s$-states penetrate the $3d$-semicore states, hence some care is necessary in treating the valence-core interactions. Thus the partial nonlinear core-corrections were included in the pseudopotential. The Hellmann-Feynman forces exerted on the atoms and the stresses acting on the unit cell are also calculated. For the calculations of the pressure dependence of the structural parameters, elastic constants and the Γ-point phonon frequencies we have used the elementary unit cell with 6 to 36 atoms depending on symmetry. For the phonon dispersion relations, we used $2\times2\times2$ supercells with 48 atoms. The $2\times2\times2$ supercell allows us to check the dynamical stability of the system by verifying that all phonon frequencies are real. Because of very small energy differences between phases in the vicinity of the phase-transition points, we put particular attention to the convergence of the energy with respect to the electronic kinetic-energy cutoff and the integration over the Brillouin zone. A plane-wave basis set with 494-eV energy cutoff was used to expand the electronic wave functions at special k-points mesh generated by $4\times4\times4$ and $2\times2\times2$ Monkhorst Pack scheme for the $1\times1\times1$ and $2\times2\times2$ supercells, respectively. The applied convergence allowed us to obtain residual forces exerted on atoms being less than 0.0002 eV/Å. In the vicinity of the continuous phase transition, however, the energy differences between the phases appear to be too small with respect to the convergence obtained by the above methods. Thus, we turned the minimization of the electronic degrees of freedom in the vicinity of the transition point, from the iterative matrix diagonalization based on the minimization of the norm of the residuum vector in each eigenstate, to the conjugate gradient method. The latter is proven to be globally convergent.

III. PHASE TRANSITIONS

The calculated structural parameters of the stable phases of GeO_2 are given in Table I. They have been obtained as a result of the minimization of the supercell ground-state energies with respect to the electronic states and ionic configurations. In Table II the lattice parameters of the rutile-type phase are compared with available experimental data and

TABLE II. Comparison of measured and calculated lattice parameters of rutile-type phase $P4_2/mnm$ of GeO_2. Lattice constants are in Å. Oxygen position is O:(x,x,0).

Lattice constants	Present	Experiment[a]	Experiment[b]	Calculation[c]	Calculation[d]
a	4.3838	4.4066	4.4066	4.3515	4.5623
c	2.8637	2.8619	2.8619	2.8628	2.7474
x	0.3059	0.3059	0.3060	0.3060	0.3032

[a]Reference 15.
[b]Reference 14.
[c]Reference 17.
[d]Reference 19.

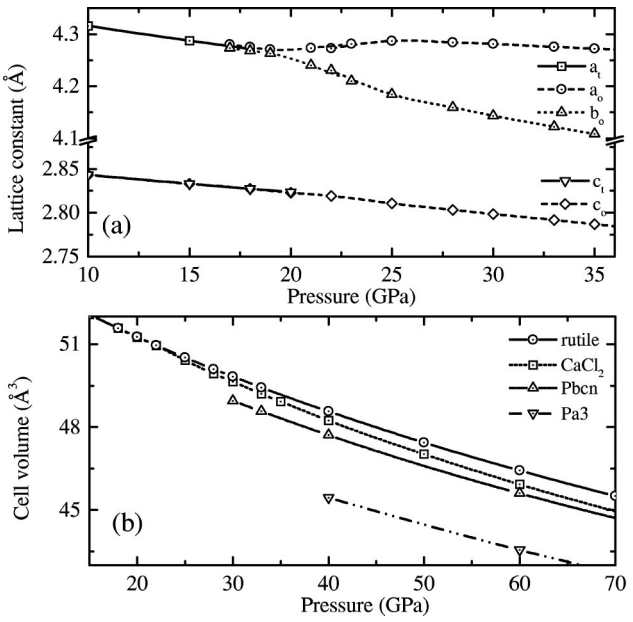

FIG. 1. Pressure dependence of the lattice parameters of tetragonal rutile-type and orthorhombic $CaCl_2$-type phases of GeO_2. (a) The lattice constants, (b) the unit cell volume V. In (b) the pressure dependence of volumes for all calculated phases in the sequence are given. For $Pbcn$ and $Pa\bar{3}$ phases half of the volume of the unit cell is shown.

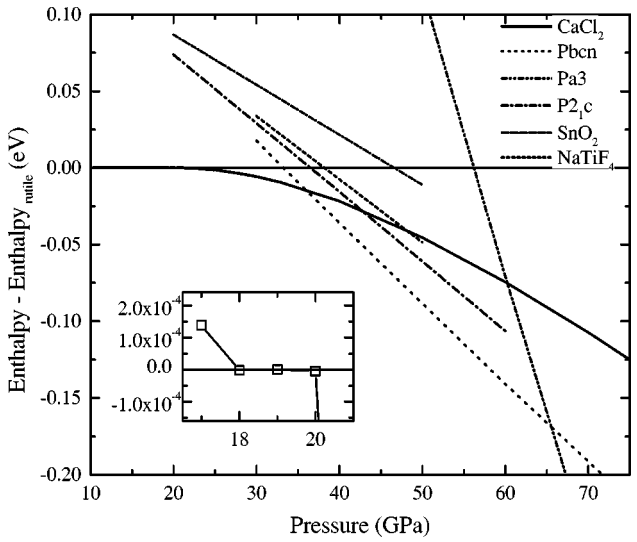

FIG. 2. The difference of Gibbs free energy $(E+PV)$ of the $CaCl_2$, $Pbcn$ $Pa\bar{3}$, and other considered phases with respect to the rutile-type phase as a function of pressure. The rutile-type phase has been optimized under constraints of $P4_2/mnm$ space group. The inset shows the energy differences between tetragonal and orthorhombic phases in the vicinity of the second-order phase transition point. Axis labels in the inset are the same as on the main axes.

other calculations. A good agreement within a 0.5% interval is found.

A. Rutile-type—$CaCl_2$-type phase transition

The cell parameters and atomic positions of the tetragonal rutile-type and orthorhombic $CaCl_2$-type structures were optimized for several pressures up to 80 GPa. One could preserve the tetragonal phase for pressures far above the transition point provided the symmetry constraints of the $P4_2/mnm$ space group are imposed.

The resulting lattice parameters are presented in Fig. 1(a). One can see that above around 19 GPa the square base of the tetragonal unit cell transforms smoothly to the rectangular one, consistent with an orthorhombic symmetry. On the contrary, at pressures below 19 GPa the orthorhombic phase always relaxes spontaneously to the tetragonal structure. The smaller unit cell volume of the orthorhombic-type structure above 19 GPa, as seen in Fig. 1(b), indicates that the $CaCl_2$-type structure is more densely packed than rutile-type structure. At this point, it is worth to mention that the ionic optimization methods like quasi-Newton and conjugate gradient, appear to fail in the definite estimation of transition pressure by the unit cell relaxation. Since energy differences between both the phases tend to become very small, already 2 GPa away from the phase transition (less than ~ 0.001 eV), the inaccuracy of the lattice constants in this pressure range increases. The inaccuracy of about 1% seem to be impossible to overcome in this region. The changes of the cell parameters and the cell volume are almost continuous, and that suggests that this phase transition is quite close to the second order. The axial ratio c/a increases linearly as suggested also by the experiment.[6]

The precise information about the stability of GeO_2 can be deduced from the pressure dependence of the Gibbs free energy. In Fig. 2 the differences of the Gibbs free energies between $CaCl_2$, $Pbcn$, and $Pa\bar{3}$-type phases and some other phases as proposed in Refs. 8 and 7 with respect to the rutile-type phase are depicted. Above 20 GPa $CaCl_2$-type structure becomes energetically more favorable. However, as seen in the inset, in the energy range between 18 and 20 GPa the energy differences are too small to distinguish the absolute stability between phases. Below we present another method to estimate accurately the transition pressure. Our lattice constants, volume and free energy behavior give similar phase transition pressure around 19.0 GPa and this value is lower than the experimental one at 26.7 GPa (Ref. 16) and ambient temperature. The result is not surprising, since it is well known that in some cases density functional theory calculations at $T=0$ K, could underestimate the transition pressures for about 30%.

B. $CaCl_2$-type to α-PbO_2-type phase transition

Neither the Hartree-Fock calculations[17] nor the parametrized potential calculations[18] of germanium dioxide deal with a possible $CaCl_2$–α-PbO_2 transformation. However, in analogy to SiO_2 and SnO_2, such phase transition should exist in GeO_2. From the pressure dependence of the Gibbs free energy presented in Fig. 2 we find that at the pressure of 36 GPa a structural change to the α-PbO_2-type phase with the space group $Pbcn$ $(Z=4)$ occurs. This phase transition involves large atomic rearrangements with respect to the

$CaCl_2$-type structure. The **c** lattice vector is approximately doubled. The finite volume change [Fig. 1(b)] at the transition point, indicates its first-order character. The predicted structural parameters of the $Pbcn$ phase at 40 GPa are given in Table I. Experimentally[2,8] the space group of α-PbO_2-type phase has been determined as $Pnc2$. The $Pbcn$ structure can be mapped onto $Pnc2$ lattice by a simple axis permutation and the shift of the unit cell origin.[7] In fact our calculated cell parameters and atomic positions at pressures of 40–60 GPa could be equally well described by $Pnc2$ or $Pbcn$ space group.

Within the stability range of $Pbcn$ phase the series of competitive phases may exist for SiO_2 as proposed by Teter *et al.*[7] Among them we consider for GeO_2 the orthorhombic phases of 4×4 SnO_2 ($Pbcn$,$Z=12$), 3×3 $NaTiF_4$ ($Pbcn$,$Z=8$) and the monoclinic 3×2 $P2_1/c$ ($Z=6$) since they seem to be of the main importance. We have checked the possible stability of those phases, as shown in the Fig. 2. The lattice parameters of the orthorhombic tin dioxide-type phase at 50 GPa are $a=4.03$, $b=5.06$, $c=13.79$. Those of $NaTiF_4$-type are: $a=4.03$, $b=5.06$, $c=9.17$, and the monoclinic $P2_1/c$-type at 40 GPa $a=7.77$, $b=4.10$, $c=5.12$, $\beta=117^044'$. We checked that the phase of baddelyite (seven coordinated Ge) is even less stable. All the above results indicate that the α-PbO_2-type $Pbcn$ phase is the most stable one in the pressure range from 36 to 65.5 GPa.

C. α-PbO_2-type to pyrite-type phase transition

The calculations performed in Ref. 17 for GeO_2 predict that a pyrite structure with space group $Pa\bar{3}$ should become stable above 60 GPa. Our calculations (see Fig. 2) indicate that the cubic phase becomes energetically more favorable with respect to the rutile-type one at pressures above 56 GPa. From the interpolation of Gibbs free energies (Fig. 2), we estimate that the $Pbcn$ phase should transform to the cubic one at about 65.5 GPa. The transformation is accompanied by an abrupt volume change [Fig. 1(b)], hence the phase transition is of the first order. The structural parameters of the GeO_2 phase with the pyrite structure at 70 GPa are given in Table I.

D. Internal structural changes from 0 GPa to 70 GPa

With the comfort of the reader in mind, we go through the descriptive presentation of the structural transition in GeO_2. The structural changes in silica are described by the mutual rearrangements of SiO_6 octahedra; for a detailed discussion see, e.g., Teter *et al.*[7] Rutile-type GeO_2 is composed of distorted GeO_6 octahedrons aligned along the **c** direction, which share corners in (a,b) plane and their edges along **c**. The octahedrons possess two slightly different Ge-O bond lengths (1.870 Å and 1.896 Å) at 0 GPa and consequently different O-O separations. As is well known, the primary response of the system to the increasing pressure should affect the weakest bonds. Thus, similar to SiO_2 we observe a contraction of the oxygen separations, connected with rotations of oxygens around **c** axis. The Ge atoms remain in their host positions. The phase transition to the $CaCl_2$ type occurs when the rotation of semirigid GeO_6 octahedron breaks the tetragonal symmetry. This symmetry breaking is connected to distortions of O-Ge-O bond angles. These distortions increase within $CaCl_2$-type phase, but the Ge ions reside at their previous equilibrium positions. When the distortions affect the germanium atoms, the alignment of the octahedra along the **c** direction is lost and a denser arrangement in the α-PbO_2 structure is adopted. Further increase of the pressure leads to the cubic phase, in which unlike in the other phases, there is no edge sharing between octahedra. The oxygen atoms are rather shared between vertices of three octahedra. The structures are shown in Fig. 3.

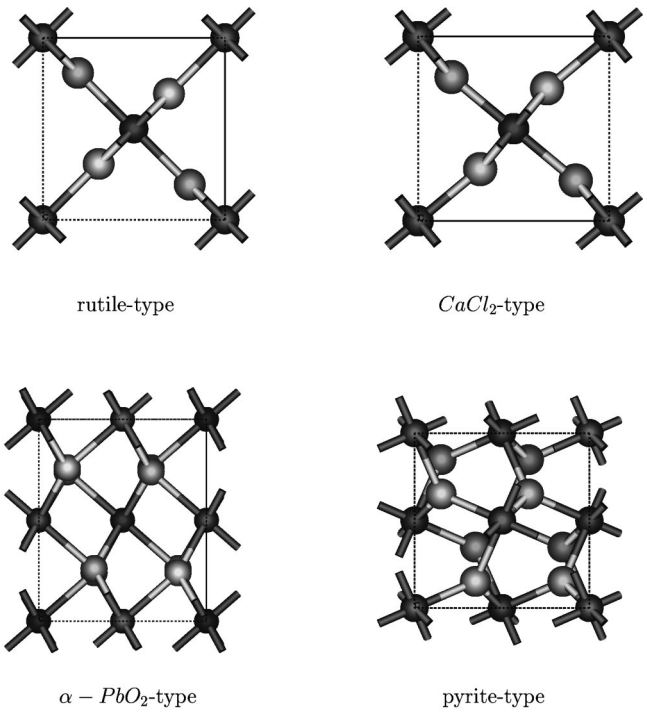

FIG. 3. Schematic plot of the top view of the unit cells of considered phases. Bright spheres represent oxygen.

IV. PHONON FREQUENCIES AND SOFT MODES

The phonon dispersion relations give a criterion for the crystal stability and indicate, through soft modes, possible structural changes. If all phonon frequencies $\omega^2(\mathbf{k})$ are positive, the crystal is at least locally stable. Thus, we calculated the phonon dispersion relations of rutile-type phase of GeO_2 at zero pressure, and of the $CaCl_2$-type structure at 30 GPa, and all phonon square frequencies proved to be positive. The phonon dispersion relations were determined by the direct method[24–27,12] using the optimized $2\times2\times2$ supercell. The Hellmann-Feynman forces were computed for the four independent displacements in the tetragonal rutile-type phase: two along **a** direction and two along **c** direction for Ge and O atoms as required by the tetragonal symmetry. The amplitude of displacement was 0.5% of the lattice constant in each direction. All calculated displacements generate 576 compo-

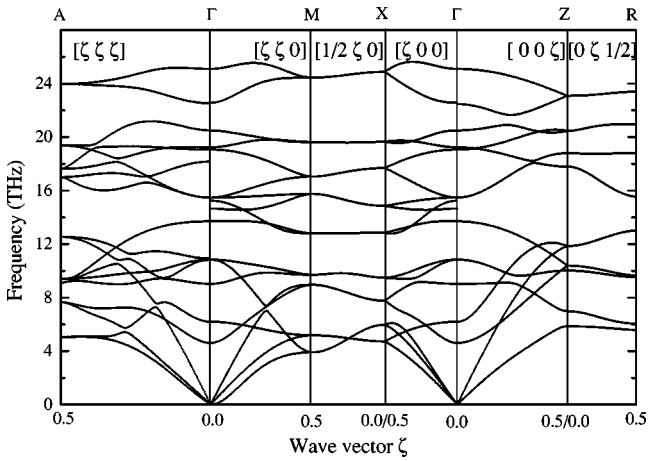

FIG. 4. Phonon dispersion relations of the rutile-type phase of GeO_2 calculated from the $2\times2\times2$ supercell.

nents of the Hellmann-Feynman forces. Making use of the symmetry of force constants following from the $P4_2/mnm$ space group, 165 independent cumulant force constants, belonging to the 34 coordination shells, are fitted by the singular value decomposition method. Those force constants are used to construct the dynamical matrix, whose diagonalization provides the phonon dispersion relations. According to the direct method, the $2\times2\times2$ supercell provides correct phonon frequencies at the Γ (0,0,0) (except longitudinal optic infrared active modes that are calculated from $1\times1\times8$ supercell), X (1/2,0,0), Z (0,0,1/2), M (1/2,1/2,0), R (1/2,0,1/2), and A (1/2,1/2,1/2) special points of the tetragonal Brillouin zone. Since the magnitude of the force constants decreases relatively fast with distance, the phonon branches, being an interpolation between special points, should be relatively well reproduced.

For polar crystals, corrections for the spurious multipole fields created by the periodic boundary conditions (expressible in terms of the Born effective charge tensor) must be added to the dynamical matrix. This leads to LO/TO splitting of infrared active modes. Since the direct method applied to $2\times2\times2$ supercell allow us to calculate TO modes only, to estimate LO frequencies we used an elongated $1\times1\times8$ supercell, and extrapolated the LO branches to zone center. Hence, we estimated effective point charges as: $Z^*(\mathrm{Ge})/\sqrt{\epsilon_\infty}=2.0$, and $Z^*(\mathrm{O})/\sqrt{\epsilon_\infty}=-1.0$. The calculated phonon dispersion curves at zero pressure for the rutile-type phase are presented in Fig. 4. In Table III we list the zone-center Raman active-mode frequencies. These modes do not depend on the nonanalytical term and are independent of the effective charge tensors.

TABLE III. Frequencies (in THz) of Raman active zone center phonon modes of the rutile-type phase of GeO_2 at 0 GPa, and $CaCl_2$-type phase at 30 GPa.

	Rutile type		$CaCl_2$ type	
Mode	Present	Expt.[a]	Mode	Present
B_{1g}	4.38	5.13	A_g	5.01
E_g	15.33		B_{1g}	15.46
A_{1g}	20.44	21.03	B_{3g}	16.59
B_{2g}	24.90	26.19	B_{2g}	17.29
			A_g	23.31
			B_{1g}	28.57

[a]Reference 16.

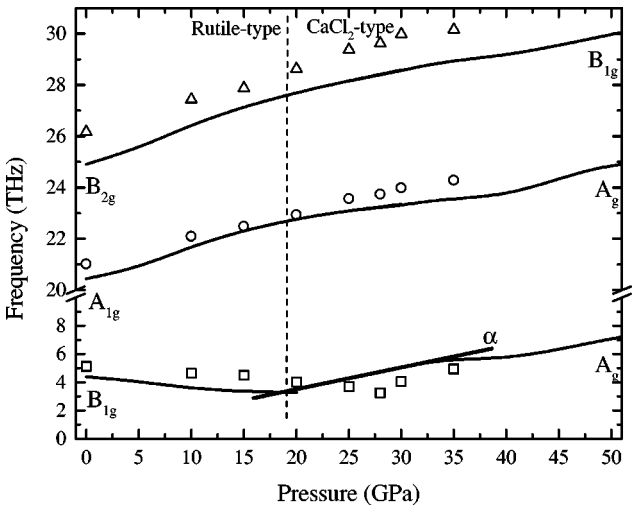

FIG. 5. The pressure dependence of the nondegenerate zone center mode frequencies of the rutile-type and $CaCl_2$-type structures of GeO_2. The experimental data are denoted by symbols. Left- and right-hand lines correspond to calculated mode frequencies of the tetragonal and orthorhombic structures, respectively. Line denoted as (α) is a guide to the eyes, suggesting the soft-mode pressure behavior in the orthorhombic phase.

The pressure dependence of the nondegenerate Raman active modes calculated using the elementary unit cell only is shown in Fig. 5. As one can see, the frequency of the B_{1g} mode decreases as the pressure is increased. On the other hand, the low-frequency mode A_g in the orthorhombic structure softens with decreasing pressure towards the phase transition point. This B_{1g} mode interacts strongly with the normal shear component of the same B_{1g} symmetry. Finally, the shear stress produces the phase transition.

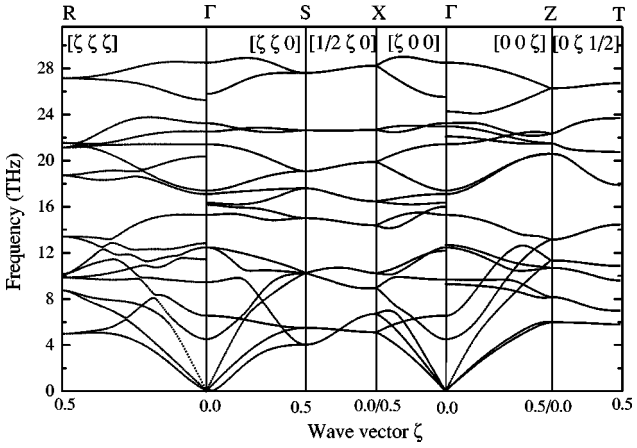

FIG. 6. Phonon dispersion relations of the $CaCl_2$-type phase of GeO_2 at 30 GPa calculated from the $2\times2\times2$ supercell.

TABLE IV. Zero-pressure elastic constants of GeO_2 compared with calculated and experimental data. The elastic constants are in GPa.

C_{ij}	Present	Experiment[a]	Calculated[b]	Calculated[c]
C_{11}	316.1	337.2	492	300
C_{12}	199.4	188.2	238	97
C_{13}	175.6	187.4	239	143
C_{33}	573.9	599.4	679	474
C_{44}	149.9	161.5	197	150
C_{66}	254.6	258.4	165	93

[a]Reference 15.
[b]Reference 28.
[c]Reference 19.

For the orthorhombic symmetry the phonon dispersion curves were calculated from the $2\times2\times2$ supercell. This symmetry requires to calculate Hellmann-Feynman forces for six independent displacements, three for Ge and three for O atom in each crystallographic directions. In Fig. 6 the phonon dispersion relations for the $CaCl_2$-type phase are presented. The effective charges were assumed to be the same as in the tetragonal phase. The mode frequencies are shown in Table III.

V. ELASTIC CONSTANTS

The pressure dependence of the elastic constants is a very important characterization of the crystals under varying pressure and/or temperature. Moreover, the change of the elastic constants at the transition point may drastically influence the macroscopic properties, such as the velocity of sound or reflective properties of the crystal.[23]

The elastic constants of the rutile type and $CaCl_2$ phases were determined from the computation of stresses generated by small deformations of the unit cell. Since it was previously suggested that phase transition from the rutile type to the $CaCl_2$ type results from strong coupling of the soft B_{1g} mode to the lattice strains, we allowed the simultaneous atomic relaxation. For each pressure, several strains of the amplitude up to 1% were applied. Then the elastic constants were determined at the appropriate limit of zero strain.

The particular direction of the unit cell deformation depend on the symmetry of each phase and the number of independent elastic constants—ranging from six for tetragonal phase to nine for orthorhombic one. The elastic constants of the tetragonal rutile-type phase are presented in Table IV and are compared with the experimentally measured[15] ones and calculated by different methods.[19,28] One can notice fairly good agreement of the *ab initio* results with the experimental values. The calculated pressure dependence of elastic constants are depicted in Fig. 7. Generally, the elastic constants change monotonically with pressure. However, the shear modulus c_{11}-c_{12} of rutile-type phase, Fig. 7(b), connected with the rotation of the oxygen octahedron, decreases with the pressure. Interpolation of c_{11}-c_{12} leads to zero at about 18.7 GPa, which implies that this is the phase transition pressure. Similarly the pressure behavior of the shear modulus $(c_{11}+c_{22})$-$2c_{12}$ of the orthorhombic phase $Pbcn$ also softens as approaching transition pressure from the high-pressure side. The observed behavior is consistent with that calculated by Karki *et al.*[23,29] The transition pressure estimated from the pressure dependence of the elastic constants is consistent with the value of 19 GPa elucidated from the structural changes and the 19 GPa obtained from the softening of the Raman B_{1g} mode.

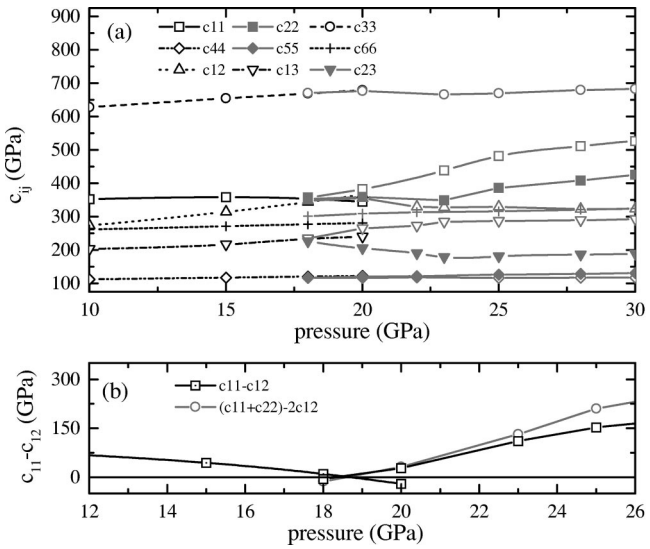

FIG. 7. (a) The pressure dependence of the elastic constants of rutile-type and $CaCl_2$ phases of GeO_2. The same symbols apply accordingly in subsequent phases. (b) The shear $c_{11}-c_{12}$ and $(c_{11}+c_{22})-2c_{12}$ for orthorhombic phase, responsible for the second-order ferroelastic phase transition, as a function of pressure.

VI. CONCLUSION

To summarize what we have calculated, within a density functional theory approach, the following series of pressure induced structural phase transitions in GeO_2 were observed: rutile$\Rightarrow$($\sim$19 GPa)$\Rightarrow$$CaCl_2$$\Rightarrow$(36 GPa)$\Rightarrow$$\alpha$-$PbO_2$$\Rightarrow$(65.5 GPa)$\Rightarrow$$Pa\bar{3}$ (pyrite). The first transition at 19 GPa is close to the second order as suggested by the lattice-constants changes and the Gibbs free energy behavior. The normal mode analysis indicate a softening of the B_{1g} Raman active mode that is strongly coupled to the shear mode responsible for the rutile-$CaCl_2$-type phase transition. Indeed, the B_{1g} soft mode eigenvector involves the rotation of SiO_6 octahedra around c axis and resembles the oxygen displacements in the orthorhombic phase with respect to their positions in the tetragonal phase. The next two phase transitions are of the first order and the phase transition to the $Pbcn$ structure occurs at 36 GPa, while the subsequent transition from $Pbcn$ to the pyrite $Pa\bar{3}$ structure occurs at 65.5 GPa. Both phases contain four formula units in the unit cell. The concurrent phases proposed for silica are less stable in this pressure range. The elastic constants changes continuously with pres-

sure, exhibiting softening in the vicinity of the second-orderphase transition. The above predicted sequence of transformations is in one to one correspondence to the sequence of transitions predicted for silica, however, these in GeO_2 occur at considerably lower pressures. Our results lead to a better understanding of the analogy between germanium dioxide and silica and might provide hints for further experimental investigations.

ACKNOWLEDGMENTS

We thank Y. Kawazoe and Z. Q. Li for turning our attention to the germanium dioxide problem. The discussions with W. Schranz are kindly acknowledged. The authors thank ACK-Cyfronet, Kraków for the computing facilities. The present work was partially supported by the State Committee of Scientific Research (KBN), Grant No. 2PO3B 069 20.

[1] K. J. Kingma, R. E. Cohen, R. J. Hemley, and H-K. Mao, Nature (London) **374**, 243 (1995).
[2] L. S. Dubrovinsky, S. K. Saxena, P. Lazor, R. Ahuja, O. Eriksson, J. M. Wills, and B. Johansson, Nature (London) **388**, 362 (1997).
[3] D. Andrault, G. Fiquet, F. Guyot, and M. Hanfland, Science **282**, 720 (1998).
[4] A. B. Belonoshko, L. S. Dubrovinsky, and N. A. Dubrovinsky, Am. Mineral. **81**, 785 (1996).
[5] Th. Demuth, Y. Jeanuoine, J. Hafner, and J. G. Angyan, J. Phys.: Condens. Matter **11**, 3833 (1999).
[6] E. Philippot, D. Palmer, M. Pintard, and A. Goiffon, J. Solid State Chem. **123**, 1 (1996).
[7] D. M. Teter, R. J. Hemley, G. Kresse, and J. Hafner, Phys. Rev. Lett. **80**, 2145 (1998).
[8] B. B. Karki, M. C. Warren, L. Stixtrude, G. J. Ackland, and J. Crain, Phys. Rev. B **55**, 3465 (1997).
[9] C. Lee and X. Gonze, J. Phys.: Condens. Matter **7**, 3693 (1995).
[10] C. Lee and X. Gonze, Phys. Rev. B **56**, 7321 (1997).
[11] J. Haines and J. M. Léger, Phys. Rev. B **55**, 11 144 (1997).
[12] K. Parlinski and Y. Kawazoe, Eur. Phys. J. B **13**, 679 (2000).
[13] J. Haines, J. M. Léger, and O. Schulte, Science **271**, 629 (1996).
[14] A. A. Bolzan, B. Fong, J. B. Kennedy, and Ch. J. Howard, Acta Crystallogr., Sect. B: Struct. Sci. **B53**, 373 (1997).
[15] H. Wang and G. Simmons, J. Geophys. Res. **78**, 1262 (1973).
[16] J. Haines, J. M. Léger, C. Chateau, R. Bini, and L. Ulivi, Phys. Rev. B **58**, 1 (1998).
[17] L. H. Jolly, B. Silvi, and P. D'Arco, Eur. J. Mineral. **6**, 7 (1994).
[18] M. Akaogi, T. Suzuki, R. Kojima, T. Honda, E. Ito, and I. Nakai, Geophys. Res. Lett. **25**, 3635 (1998).
[19] R. D. Oeffner and S. R. Elliott, Phys. Rev. B **58**, 14 791 (1998).
[20] A. R. George and C. R. A. Catlow, J. Solid State Chem. **127**, 137 (1996).
[21] G. Kresse and J. Furthmüller, VASP code, Vienna, 1999; Comput. Mater. Sci. **6**, 15 (1996); Phys. Rev. B **54**, 11 169 (1996).
[22] G. Kresse and J. Hafner, Phys. Rev. B **47**, 558 (1993); **49**, 14 251 (1994).
[23] B. B. Karki, L. Stixrude, and J. Crain, Geophys. Res. Lett. **24**, 3269 (1997).
[24] G. Kresse, J. Furtmüller, and J. Hafner, Europhys. Lett. **32**, 729 (1995).
[25] K. Parlinski, Z. Q. Li, and Y. Kawazoe, Phys. Rev. Lett. **78**, 4063 (1997).
[26] G. Kern, G. Kresse, and J. Hafner, Phys. Rev. B **59**, 8551 (1999).
[27] K. Parlinski, Software PHONON, 1999.
[28] T. Tsuchiya, T. Yamanak, and M. Matsui, Phys. Chem. Miner. **25**, 94 (1998).
[29] B. B. Karki, G. J. Ackland, and J. Crain, J. Phys.: Condens. Matter **9**, 8579 (1997).